Hydrogen engines numerical modeling

N. N. Smirnov V. F. Nikitin Yu. G. Phylippov
ebifsun1@mech.math.msu.su

Abstract

Hydrogen being an ecological fuel is very attractive now for engines designers. It is already actively used in rocket engines. There exist plans to use hydrogen in pulse detonation engines. However, peculiarities of hydrogen combustion kinetics, the presence of zones of inverse dependence of reaction rate on pressure, etc. prevent from wide use of hydrogen engines. Computer aided design of new effective and clean hydrogen engines needs mathematical tools for supercomputer modeling of hydrogen - oxygen components mixing and combustion gas dynamics.

The paper presents the results of developing verification and validation of mathematical model and numerical tool making it possible to simulate unsteady processes of ignition and combustion in engines of different types.

1 Introduction

Rocket engines using hydrogen-oxygen mixture have the following peculiarity. On injecting liquid components fuel (hydrogen) having much lower critical temperature comes pre-evaporated and pre-heated in combustion chamber, while oxygen could be liquid then evaporating inside the chamber. Thus contrary to most types of engines hydrogen engine has an inverse mixture entering combustion chamber, in which fuel is gaseous and oxidant is liquid. However, taking into account rather low critical temperatures for both components estimates based on models developed in [1-3] show, that phase transition will take place in an order of magnitude faster then for hydrocarbon fuels. That provides the reason to use one phase model as a first order of approximation. Onset of detonation being very dangerous for classical RAM engines could, however, serve the basis for creating new generation of engines - pulse detonating engines (PDE) [4, 5]. For this issue the problems of detonation onset, decay and deflagration to detonation transition should be simulated quite accurately, because these processes strongly depend on inlet conditions, mixture composition and geometrical characteristics of combustion chamber [6-8].

Hydrogen chemistry modeling is rather complicated because regular kinetic mechanisms have hundreds stages. Many reduced kinetic mechanisms were developed. However, peculiarities of hydrogen combustion kinetics, the presence of zones of inverse dependence of reaction rate on pressure, makes developing reduced mechanisms a very difficult task, which was studied by many researchers [9-14]. In the present paper kinetic models developed based on methodology [15] will be used. The validation of these models will be performed based on experimental investigations of ignition delay times being functions of pressure, temperature and mixture composition [16, 17].

2 Mathematical model

Numerical investigations of the DDT processes were performed using the system of equations for the gaseous phase obtained by Favre averaging of the system of equations for multicomponent multiphase media. The modified k-epsilon model was used. To model temperature fluctuations the third equation was added to the k-epsilon model to determine the mean squared deviate of temperature [7, 8]. The production and kinetic terms were modeled using the Gaussian techniques [18, 19].

The governing equations for the averaged values of parameters look as follows:

$$\partial_t(\rho) + \nabla \cdot (\rho \underline{u}) = 0, \tag{1}$$

$$\partial_t(\rho Y_k) + \nabla \cdot (\rho \underline{u} Y_k) = -\nabla \cdot \underline{I_k} + \dot{\omega}_k, \tag{2}$$

$$\partial_t(\rho \underline{u}) + \nabla \cdot (\rho \underline{u} \otimes \underline{u}) = \rho \underline{g} - \nabla p + \nabla \cdot \tau, \tag{3}$$

$$\partial_t(\rho E) + \nabla \cdot (\rho \underline{u} E) = \rho \underline{u} \underline{g} - \nabla \cdot p \underline{u} - \nabla \cdot \underline{I_q} + \nabla \cdot \tau \underline{u}. \tag{4}$$

The equations (1-4) include mass balance in the gas phase, mass balance of k-th component, momentum balance and energy balance respectively. We have the following relationships between the terms in the equations (1-2): $\sum_k Y_k = 1$, $\sum_k \underline{I_k} = 0$, $\sum_k \dot{\omega}_k = 0$. The state equations for gaseous mixture are the following: $p = \rho \frac{R_g}{m} T = \rho R T \sum_k \frac{Y_k}{W_k}$, $E = \sum_k Y_k (c_{vk} T + h_{0k}) + \frac{\underline{u}^2}{2} + k$. The turbulent heat flux $\underline{I_q}$ in the equation (4) is a sum of two terms: $\underline{I_q} = \underline{J_q} + \sum_k (c_{pk} T + h_{0k}) \underline{I_k}$, where $\underline{J_q}$ could be interpreted as turbulent conductive heat flux. The eddy kinematic viscosity ν^t is expressed according to k-epsilon model as $\nu^t = C_\mu \frac{k^2}{\varepsilon}$. The turbulent fluxes were modeled in the following way:

$$\tau = (\mu + \rho \nu^t)(\nabla \cdot \underline{u} + \nabla \cdot \underline{u}^T - \frac{2}{3}(\nabla \cdot \underline{u}) U) - \frac{2}{3} \rho k U, \tag{5}$$

$$\underline{I_k} = -\rho (D + \frac{\nu^t}{\sigma_d}) \nabla Y_k, \underline{J_q} = -(\lambda + \sum_k c_{pk} Y_k \rho \frac{\nu^t}{\sigma^t}) \nabla T. \tag{6}$$

The k-th component mass origination rate $\dot{\omega}_k$ was calculated as a sum of mass production rates ω_{kj} in each n-th chemical reaction taking place in a gaseous phase. The term responsible for chemical transformations, $\dot{\omega}_k$ is very sensitive to temperature variations, as it is usually the Arrhenius law type function for the reactions' rates. Let us regard the temperature being a stochastic function T with mean $\overline{T}$ and mean squared deviate $\theta = \overline{T'T'}$ .The model was closed then by the equations for k, θ and ϵ :

$$\partial_t(\rho k) + \nabla \cdot (\rho \underline{u} k) = \nabla \cdot ((\mu + \rho \frac{\nu^t}{\sigma_k}) \nabla k) + \frac{\tau^t}{\nabla \cdot \underline{u}} - \rho \varepsilon, \tag{7}$$

$$\partial_t(\rho \varepsilon) + \nabla \cdot (\rho \underline{u} \varepsilon) = \nabla \cdot ((\mu + \rho \frac{\nu^t}{\sigma_\varepsilon}) \nabla \varepsilon) + \frac{\varepsilon}{k} (\frac{C_{1\varepsilon} \tau^t}{\nabla \cdot \underline{u}} - C_{2\varepsilon} \rho \varepsilon), \tag{8}$$

$$\partial_t(\rho \tilde{c_p} \theta) + \nabla \cdot (\rho \underline{u} \tilde{c_p} \theta) = \nabla \cdot ((\lambda + \sum_k c_{pk} Y_k \rho \frac{\nu^t}{\sigma^k}) \nabla \theta) + P_\theta + W_\theta - D_\theta, \tag{9}$$

where the production terms P_θ, W_θ and the dissipation term D_θ were determined by the following formulas:

$$P_\theta = 2\rho \sum_k c_{pk} Y_k \frac{\nu^t}{\sigma^k} (\nabla T)^2, W_\theta = -\sum_k \overline{\dot{\omega}_k' T'} h_{0k}, \tag{10}$$

$$D_\theta = C_g \rho \sum_k c_{pk} Y_k \frac{\varepsilon}{k} \frac{\theta}{\theta_m - \theta}, \tilde{c_p} = \sum_k c_{pk} Y_k. \tag{11}$$

In deriving the production W_θ due to chemistry the Arrhenius law for chemical transformations was assumed. To calculate the averaged term $\dot{\omega}_k$ the Gaussian quadrature technique was applied:

$$\overline{T' A(T)} = \theta \frac{A(\overline{T} + \sqrt{3\theta}) - A(\overline{T} - \sqrt{3\theta})}{2\sqrt{3\theta}}. \tag{12}$$

The dissipation function D_θ was chosen in the form (10-11) to satisfy the rule that the squared temperature deviate cannot exceed its maximal possible value θ_m , because the value of $T = \bar{t} + T'$ cannot be negative. However, production terms do not grant the presence of such a boundary. To guarantee it we incorporate the multiplier $\frac{1}{\theta_m - \theta}$ into the dissipation term (the other multipliers are standard, see [19]). In order to estimate the value of θ_m , we should take into account that in experiments [18] the probability for the deviate value to exceed 2 times the mean deviate value is less than 1% for the normal distribution. Also, we should take into account that the mean temperature deviate in experiments [18] did not exceed half of the maximal mean temperature. With this, we estimate θ_m as follows: $\theta_m = \frac{\overline{T}^2}{4}$. The dissipation constant C_g in (10) could be determined based on the experiments [18]: $C_g = 2.8$.

The constants in (7-11) take the following standard values: $C_\mu = 0.09$, $C_{1\varepsilon} = 1.45$, $C_{2\varepsilon} = 1.92$, $\sigma_d = 1$, $\sigma_t = 0.9$, $\sigma_k = 1$, $\sigma_s = 1.3$.

The boundary conditions for turbulent parameters k, ϵ, θ are constructed according to the wall laws [5]:

$$k = 0, \frac{\partial \theta}{\partial \underline{n}} = 0, \frac{\partial \varepsilon}{\partial \underline{n}} = 0, \tag{13}$$

where $\underline{n}$ is the normal vector to the wall. To take into account the wall damping effect the coefficients of the original turbulence model are modified in accordance with the Lam-Bremhorst low Reynolds models [21]:

$$C_\mu = C^0_\mu f_\mu, C_{1\varepsilon} = C^0_{1\varepsilon} f_1, C_{2\varepsilon} = C^0_{2\varepsilon} f_2,$$

where $0 < f\mu \leq 1, f_1 \geq 1, 0 \leq f_2 \leq 1$ are positive functions which depend on two local Reynolds numbers $R_1 = \frac{k^2}{\nu\epsilon}$, $R_y = \sqrt{k}\frac{y}{\nu}$, where y is a distance from the nearest wall. For the Lam-Bremhorst low Reynolds $k-\varepsilon$ model the functions are determined in the following way:

$$f_\mu = (1 - \exp(-0.0165 R_y))^2 (1 + \frac{20.5}{R_t}),$$

$$f_1 = 1 + (\frac{0.05}{f_\mu})^3, f_2 = 1 - \exp(-R_t^2).$$

The generalized reaction mechanism looks as follows:

$$\sum_{k=1}^{N_C} \nu'_{rk} A_k (+M_r) \Leftrightarrow \sum_{k=1}^{N_C} \nu"_{rk} A_k (+M_r), r = 1...N_R,$$

where N_R - number of chemical reactions; N_C - number of species; ν_{rk} - elements of the matrix of stoicheometric coefficients; ω_r - r-th reaction rate; $(+M_r)$ - characterizes the effect of a third body in r-th reaction.

The rates of species origination are supposed to yield the Arrhenius law and the acting masses law. With multiple reactions, the origination rates are split into elementary parts:

$$\dot{\omega}_k = \sum_{r=1}^{N_R} \omega_{kr},$$

where ω_{kj} is the k-th species origination rate per volume due to j-th reaction.

The molar rate of k-th component production due to chemistry: $\hat{\omega}_k = \frac{\dot{\omega}_k}{W_k}$, $\hat{\omega}_k = \sum_{r=1}^{N_R} \nu_{rk}\omega r$, $\nu_{rk} = \nu"_{rk} - \nu'_{rk}$.

Reaction rate coefficient for brutto mechanisms and elementary reactions looks as follows:

$$\omega_r = (\sum_{j=1}^{N_C} \gamma_{rj} X_j)^{m_r} (k_r^D \prod_{k=1}^{N_C} X_k^{\alpha_{rk}} - k_r^R \prod_{k=1}^{N_C} X_k^{\beta_{rk}}),$$

where $m_r = 0$ or 1 for chemical interactions disregarding or taking into account the third body effect; γ_{rj} - coefficients accounting for components affecting third body effect (Chaperon coefficients); k_r^D, k_r^R - coefficients of direct and reverse reaction; α_{rk}, β_{rk} - power for concentration, which usually for elementary stages correspond with stoicheometric coefficients; $X_k = \frac{\rho Y_k}{W_k}$ - molar concentration per volume unit. For irreversible reactions one has $k_r^B = 0$.

The temperature deviation production term in the equation (9) for multiple species and reactions has the following form:

$$W_\theta = -\overline{T' \sum_{r=1}^{N_R} \sum_{k=1}^{N_C} h_k^0 \dot{\omega}_{kr}}, \tag{14}$$

where h_k^0 - chemical energy of the k-th component.

Each term ω_{kj} incorporates Arrhenius function for the j-th reaction $A_j(T)$, which is assumed to have the following form:

$$A_r(T) = \begin{cases} K_r \exp(-\frac{T_{ar}}{T}), T \geq T_{mr} \\ 0, T \leq T_{mr} \end{cases} \tag{15}$$

where K_r is the pre-exponential factor, T_{ar} is the activation temperature, T_{mr} is the minimum temperature. In order to obtain the term W_θ (14), one should find the mean values $\overline{T' A_r(T)}$ using formula (12) and then sum those terms up using formula (14). The procedure for averaging non-linear functions was described in details in [5].

The boundary of the computational domain contains the outer walls and the axis of symmetry. The walls for the case of cylindrical symmetry could be a combination of coaxial cylindrical surfaces and rings or plates orthogonal to the axis.

The boundary conditions for the gas phase are constructed in accordance with the following considerations: the walls of the cylindrical domain are thermo-insulated and non-catalytic, the velocity of gas is zero on the walls and the averaged gas motion has cylindrical symmetry. This leads to von Neumann's conditions for temperature and mass fractions of species at the walls of the cylinder (their normal derivatives are equal to zero).

The gaseous phase was supposed to contain the following set of species: H_2O, OH, H, O, HO_2, H_2O_2, O_2, H_2, N_2.

The following brutto reactions between the species were considered:

N_R	**Reaction**	**Reaction rate coefficient** k_r^D
1	$O_2 + H \Leftrightarrow OH + O$	$2.00 \cdot 10^{14} \cdot \exp(\frac{-70.3}{R_G T})$
2	$H_2 + O \Leftrightarrow OH + H$	$5.06 \cdot 10^{4} \cdot T^{2.67} \cdot \exp(\frac{-26.3}{R_G T})$
3	$H_2 + OH \Leftrightarrow H_2O + H$	$1.00 \cdot 10^{8} \cdot T^{1.60} \cdot \exp(\frac{-13.8}{R_G T})$
4	$OH + OH \Leftrightarrow H_2O + O$	$1.50 \cdot 10^{9} \cdot T^{1.14} \cdot \exp(\frac{-0.4}{R_G T})$
5	$H + H + M \Leftrightarrow H_2 + M$	$1.80 \cdot 10^{18} \cdot T^{-1.00}$
6	$O + O + M \Leftrightarrow O_2 + M$	$2.90 \cdot 10^{17} \cdot T^{-1.00}$
7	$H + OH + M \Leftrightarrow H_2O + M$	$2.20 \cdot 10^{22} \cdot T^{-2.00}$
8	$H + O_2 + M \Leftrightarrow HO_2 + M$	$2.30 \cdot 10^{18} \cdot T^{-0.80}$
9	$HO_2 + H \Leftrightarrow OH + OH$	$1.50 \cdot 10^{14} \cdot \exp(\frac{-4.2}{R_G T})$
10	$HO_2 + H \Leftrightarrow H_2 + O_2$	$2.50 \cdot 10^{13} \cdot \exp(\frac{-2.9}{R_G T})$
11	$HO_2 + H \Leftrightarrow H_2O + O$	$3.00 \cdot 10^{13} \cdot \exp(\frac{-7.2}{R_G T})$
12	$HO_2 + O \Leftrightarrow OH + O_2$	$1.80 \cdot 10^{13} \cdot \exp(\frac{+1.7}{R_G T})$
13	$HO_2 + OH \Leftrightarrow H_2O + O_2$	$6.00 \cdot 10^{13}$
14	$HO_2 + HO_2 \Leftrightarrow H_2O_2 + O_2$	$2.50 \cdot 10^{11} \cdot \exp(\frac{+5.2}{R_G T})$
15	$OH + OH + M \Leftrightarrow H_2O_2 + M$	$3.25 \cdot 10^{22} \cdot T^{-2.00}$
16	$H_2O_2 + H \Leftrightarrow H_2 + HO_2$	$1.70 \cdot 10^{12} \cdot \exp(\frac{-15.7}{R_G T})$
17	$H_2O_2 + H \Leftrightarrow H_2O + OH$	$1.00 \cdot 10^{13} \cdot \exp(\frac{-15.0}{R_G T})$
18	$H_2O_2 + O \Leftrightarrow OH + HO_2$	$2.80 \cdot 10^{13} \cdot \exp(\frac{-26.8}{R_G T})$
19	$H_2O_2 + OH \Leftrightarrow H_2O + HO_2$	$5.40 \cdot 10^{12} \cdot \exp(\frac{-4.2}{R_G T})$

Table 27: Kinetic mechanism [12].

In table 1 reactions 1 - 4 correspond to reaction exchanges involving "light" radicals O, H, OH, reactions 5 - 7 are responsible for recombination of "light" radicals, in reactions 8 - 13 "heavy" radical HO_2 is involved as well, the rest of reactions 14 - 19 are characterized by the presence of another "heavy" radical H_2O_2.

3 Verification and validation of kinetic model

Validation of the model will be performed based on the analysis of ignition delay times for hydrogen-oxygen mixtures measured experimentally for different conditions: pressure, temperature and mixture composition. Ignition delay is a notation characterizing in experiments the time interval between mixture is placed under definite conditions and active energy release beginning accompanied by temperature and pressure growth. Ignition delay are often measured in shock tube experiments behind reflected shock waves.

In our simulations all parameters should change continuously, as it could be seen from the governing system of equations. We shall determine ignition delay as a time interval within which reaction conversion rate reaches maximal value, after reaching which active conversion process begins. Calculation of ignition delay is carried out as follows. A system of ordinary differential equations of reaction kinetics is being solved. The unknown functions are densities ρ_k and temperature T :

$$\frac{\partial \rho_k}{\partial t} = \dot{\omega}_k(\rho_k, T), k = 1...N_C, (\rho e)(\rho_k, T) = (\rho e)(\rho_k^0, T^0) = (\rho e)_0. \tag{16}$$

(ρ_k^0, T^0) - initial mixture state, (ρe) - energy in a volume unit. System (16) incorporates N_C differential equations and one algebraic equation.

Initial condition ρ_k^0 is calculated based on given mixture composition, pressure p^0 and temperature T^0. Ignition delay was determined by the following criterion:

$$\tau = (t \in (0, t_{max}) : |\frac{dX_{H_2}}{dt}|_t = max). \tag{17}$$

Value t_{max} is chosen to have guaranteed combustion process in the cell.

4 Ignition delay for hydrogen - oxygen mixtures

In the present section the results of ignition delays calculations are presented for different initial conditions.

Figure 1 illustrates the ignition delays for stoicheometric hydrogen - air mixture being functions of initial pressure and temperature within the temperature range $900 \div 2100K$; pressure variation 0.1 up to 200 bar. The mixture composition was maintained constant: $[H_2] : [O_2] : [N_2] = 2 : 1 : 4$.

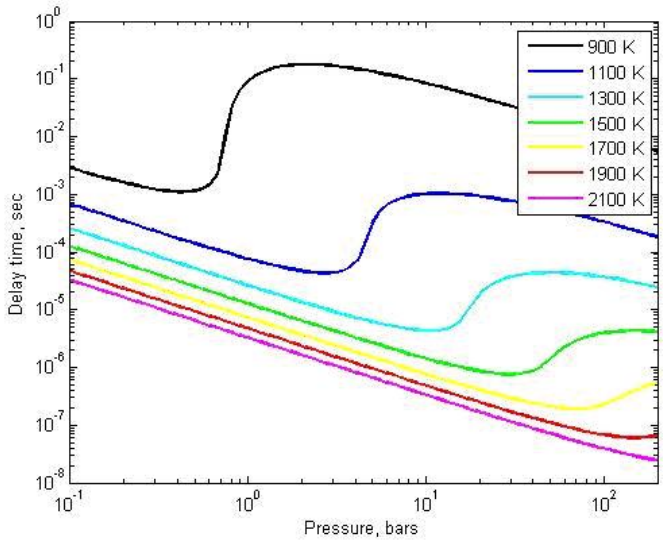

Figure 1: Ignition delays for stoicheometric hydrogen - air mixture: $[H_2] : [O_2] : [N_2] = 2 : 1 : 4$. Temperature range $900 \div 2100$ K.

As it is seen from Figure 1, ignition delay time t_{ign} is essentially non-monotonous on increasing pressure. For low pressures ignition delay decreases on increasing pressure. Then further pressure increase brings to a rapid increase of ignition delay time several orders of magnitude. Further pressure increase brings again to gradual decrease of ignition delay time. The deviation of the curve of ignition delay due to this non-monotonous behavior reaches several orders of magnitude, and it is bigger for low initial temperatures. For initial temperatures surpassing 2000 K non-monotonous behavior is already hardly noticeable within the scales present in Figure 1. However, this anomaly still exists. Deviation from straight line in a logarithmic scale decreases on increasing temperature and is shifted towards higher pressures.

The dependence of ignition delay time on initial temperature for different values of initial pressures is shpwn in Figure 2 for stoicheometric mixture of hydrogen with air. In

Figure 2 the temperature scale is linear, but the ignition delay time scale is logarithmic. Thus exponential dependence within this scale looks like a straight line.

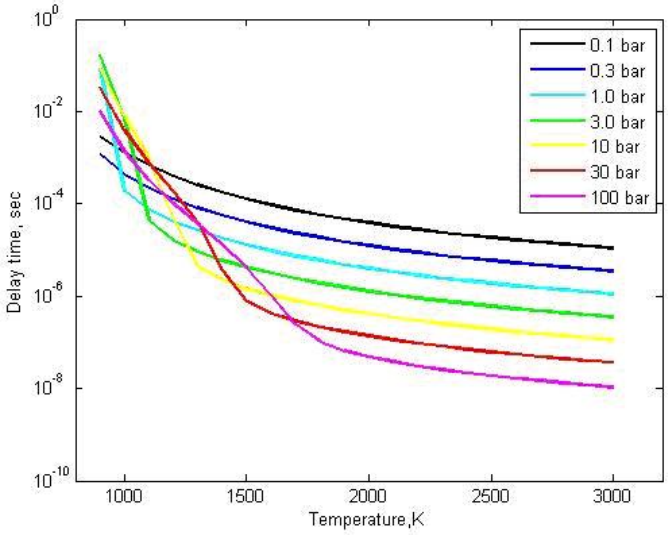

Figure 2: Ignition delays for stoicheometric hydrogen - air mixture: $[H_2] : [O_2] : [N_2] = 2 : 1 : 4$ as a function of initial temperature for different values of initial pressure as a parameter.

The next test is to study the effect of mixture composition on ignition delay time, in other words, comparing ignition delays for lean and rich mixtures of hydrogen and air. Figure 3 illustrates in a normal scale the dependence $t_{ign}(\phi)$ for initial atmospheric pressure $p = p_{ref}$ and temperature ranging $1000 \div 1200K$. Mixture composition parameter ϕ is determined as a ratio of initial molar fraction of fuel (H_2) to its stoicheometric fraction. Thus defined mixture composition parameter is less than unity $(\phi < 1)$ for lean mixtures, and greater than unity $(\phi > 1)$ for rich mixtures, $\phi = 1$ for stoicheometric mixtures. Figure 4 illustrates ignition delay time for hydrogen - oxygen mixture as a function of initial pressure for different values of initial temperature within the range $1000 \div 3000K$. Pressure varies in the interval $0.1 \div 200bar$. Mixture composition $[H_2] : [O_2] : [N_2] = 2 : 1 : 0$. As it is seen from Figure 4 ignition delay time t_{ign} dependence is qualitatively similar to that for hydrogen - air mixtures: for high temperatures the hump in the curve is an order of magnitude lower, for small temperatures the hump also exists being half an order of magnitude lower and shifted towards lower pressures. Thus one can see that there exists a definite anomalous pressure and temperature range, wherein replacing oxidizing air by pure oxygen could increase ignition delay time contrary to general tendency of ignition delay time decrease in pure hydrogen - oxygen mixtures.

Anomalous deviation from straight line in logarithmic coordinates decreases with increase of temperature and is shifted towards higher pressures. As compared with results for hydrogen - air mixtures ignition delay time for oxygen mixtures is shorter in general.

Dependence of ignition delay time on initial temperature for different pressure as a parameter for stoicheometric hydrogen - oxygen mixtures is shown in Figure 5. Temperature scale is linear, ignition delay time scale is logarithmic. Exponent looks like a straight line in such scale.

The next test is aimed at studying the effect of lean and rich mixture on ignition delay for hydrogen - oxygen mixtures. Figure 6 illustrates the dependence of ignition

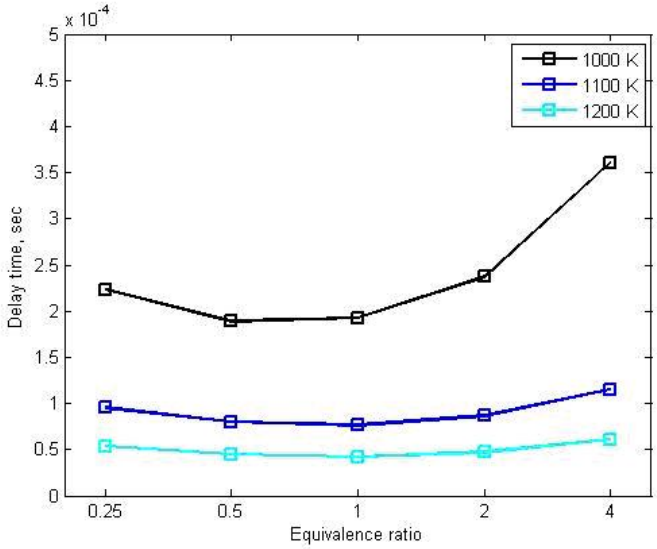

Figure 3: Ignition delays for hydrogen - air mixture as a function of its composition for different initial temperatures.

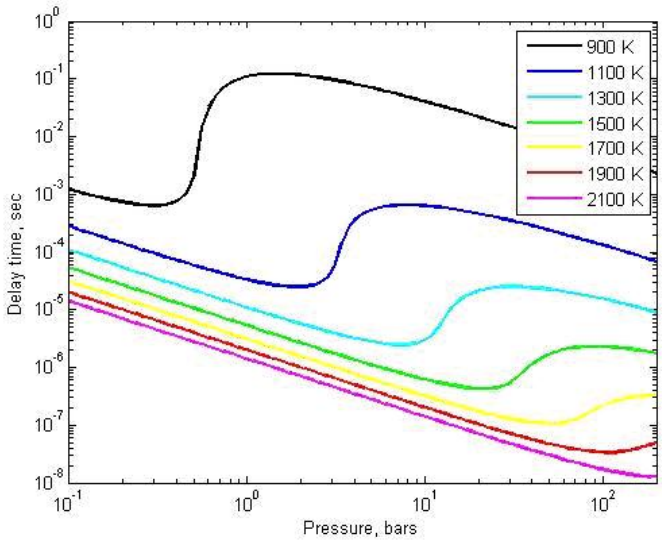

Figure 4: Ignition delay time for hydrogen - oxygen mixture as a function of initial pressure for different values of initial temperature within the range $900 \div 2100$ K. Pressure varies in the interval $0.1 \div 200$ bar. Mixture composition $[H_2] : [O_2] : [N_2] = 2 : 1 : 0$.

delay time $t_{ign}(\phi)$ on mixture composition parameter ϕ for initial atmospheric pressure $p = p_{ref}$ and temperature ranging $1000 \div 1200K$. It is seen from the Figure 6 that for low initial temperatures ($1000K$) ignition delay grows monotonously on increasing hydrogen concentration in hydrogen - oxygen mixture. Ignition delay is minimal for lean mixture, it increases for stoicheometric mixtures, and it grows rapidly for rich mixtures.

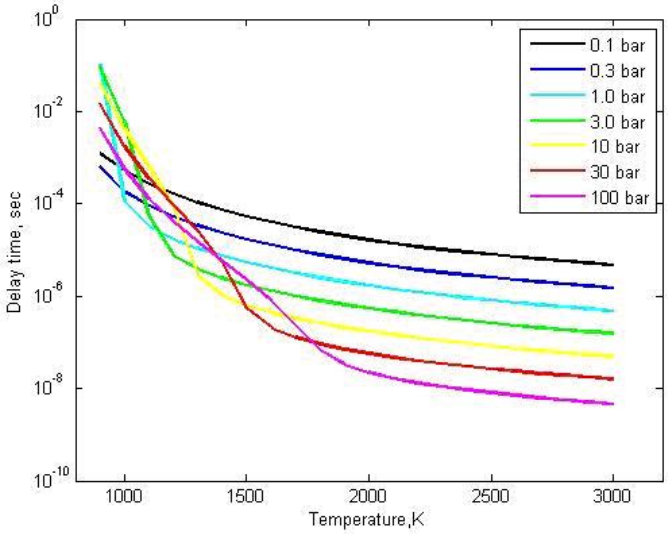

Figure 5: Dependence of ignition delay time on initial temperature for different pressure as a parameter for stoicheometric hydrogen - oxygen mixtures.

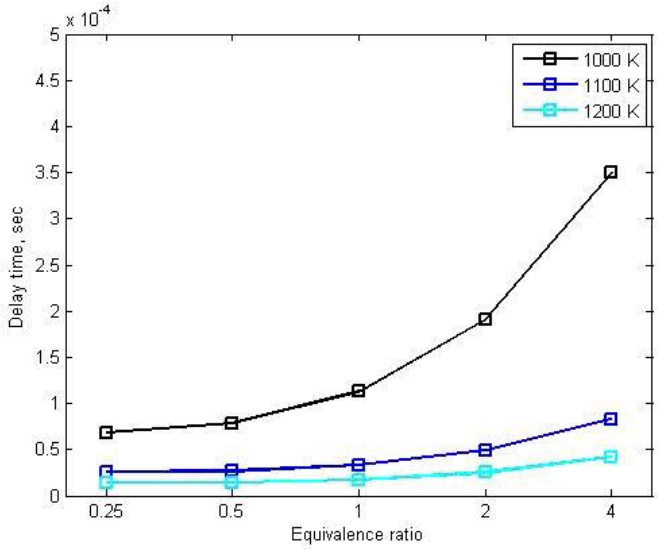

Figure 6: Ignition delay time for hydrogen - oxygen mixture as a function of mixture composition parameter.

5 Combustion mechanism validating experiments

As we have seen the dependence of ignition delay time for hydrogen - oxygen mixtures is not monotonous and has three characteristic regions.

In the first region for relatively small pressures ignition delay decreases on increasing pressure. This dependence is most well-known [10] $\tau \sim p^{-1}$ and often used in forecasts. This regions spreds up to pressures $2 \div 3$ bar the boundary moving towards pressure increase on increasing temperature.

On further increasing pressure region 1 is changed for transition region 2, wherein

ignition delay time grows on increasing pressure. The growth of ignition delay time is rather sharp: its increase is an order of magnitude takes place on increasing pressure several bars. The transition region 2 is located in the pressure range from $2 \div 3$ bar up to $5 \div 20$ bar being shifted towards higher pressures on increasing initial temperature. Despite of importance of this region there exist very few data in literature on ignition delays within this region and not all data are highly reliable [17]. Modern chemical kinetics describes this region rather qualitatively.

On increasing pressure beyond the transition region 2 ignition delay time begins decreasing again. This is region 3, wherein ignition delay dependence on pressure could be approximated by formula $\tau \sim p^{-n}, n < 1$. Pressure in this region is characteristic for that in rocket and aviation engines.

Dependence of ignition delay on temperature is always monotonous for constant pressure. Ignition delay decreases exponentially on linear increase of temperature.

Figures 7 and 8 show ignition delays variation for rich (15% hydrogen by weight) and lean (5% hydrogen by weight) mixtures. Qualitatively the curves look similar to that obtained for stoicheometric mixture, quantitatively delay time generally increases for both rich and lean mixtures as compared with stoicheometric ones (under some conditions exceptions are possible). Crosses on the figures correspond to experimental data [16]. All crosses are signed by initial values of temperature. Data was obtained from shock tube experiments. It is seen from the figures that coincidence of theoretical and experimental data is very good for high temperatures (above $1100K$), and can be assumed satisfactory for lower temperatures.

6 Detonation decay and re-initiation on entering wider chamber

The control of detonation onset in large chambers is of major importance in pulse detonating devices. The advantages of detonation mode of energy conversion over constant pressure combustion bring to the necessity of promoting the onset of detonation and shortening the pre-detonation length.

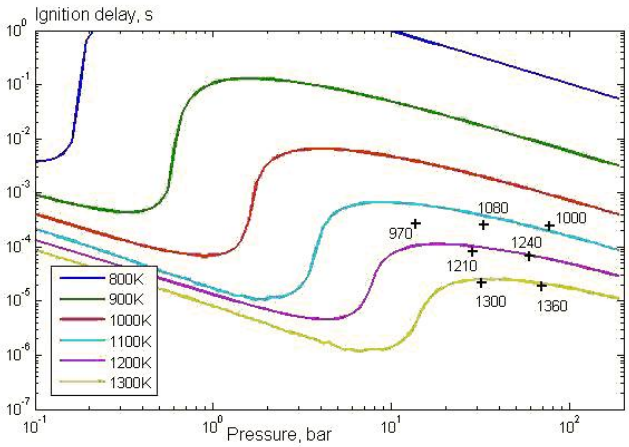

Figure 7: Ignition delay for lean mixture (5% hydrogen with oxygen by weight). Crosses correspond to experimental data.

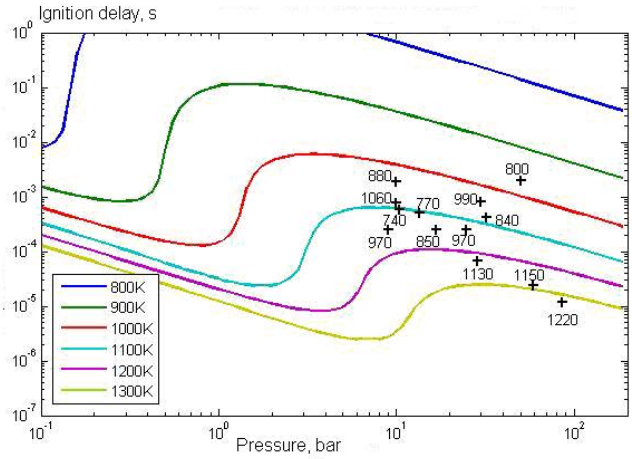

Figure 8: Ignition delay for rich mixture (15% hydrogen with oxygen by weight).

The deflagration to detonation transition (DDT) and further transmission of detonation wave into the large combustion chamber turned out to be the key factor characterizing the Pulse Detonation Engine (PDE) operating cycle. Thus, the problem of DDT control in gaseous mixtures became very acute.

The onset of detonation in large chambers could be promoted in two ways. First way is promoting DDT in the whole chamber using different turbulizing elements, such as Schelkin spiral, orifice plates, or wider cavities [4]. The method is very effective, mostly using wider cavities [5], but the predetonation length turns to be big for wide chambers [8].

Second way is promoting onset of detonation in narrow chambers, which needs much shorter pre-detonation length, and then transmitting the detonation to a wider chamber. The method is effective in terms of shortening the predetonation length, but there is a great probability the transmission of detonation could fail under certain conditions.

In the present section we'll illustrate transmission of detonation wave in a wider chamber from a narrow peripheric coaxial gap into a wide tube. On entering wider chamber decay of detonation wave begins due to divergence and decay of transverse waves. But cumulative effect on converging waves the center of the cylinder makes leading shock wave stronger, which promotes re-initiation of detonation. Of course, all scenarios are strongly dependent on reaction rate, which means on mixture composition and mixture temperature. Below Figures 9 - 11 illustrate transmission of a detonation wave from a narrow gap 20 mm width into a big cylindrical chamber 200 mm diameter. The upper part of each figure illustrates pressure fields in a cross-section, the lower part illustrates temperature fields, as the model problem was assumed to have axial symmetry.

As it is seen from the figures, transmission of detonation finally succeeds in all cases, but the fastest process takes place in a stoicheometric hydrogen - air mixture (Figure 11), which is coherent to theoretical models, because stoicheometric hydrogen - air mixtures have the shortest ignition delay time (Figure 3), which means faster reaction rate and smaller detonation cell size. However, for lean mixture (Figure 9) and diluted stoicheometric mixture (Figure 10) transmission of detonation is also successful for the present configuration, while direct transmission from 20 mm diameter tube into 200 mm diameter tube fails for both lean and diluted mixture. As it is seen from Figures 9 and 10, on entering wider chamber from a narrow gap reaction front lags behind the leading shock due to the effect of front stretch. Transverse waves travel only in the direction of expansion,

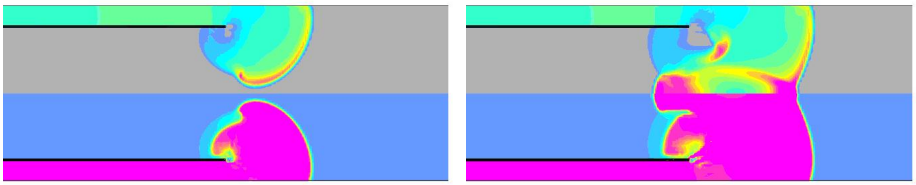

Figure 9: Transmitting detonation wave from narrow gap to cylindrical chamber $[H_2] : [O_2] : [N_2] = 1.5 : 1 : 5$.

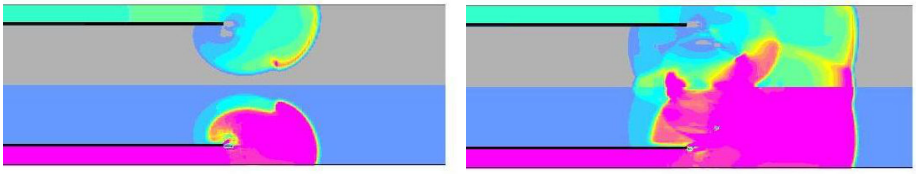

Figure 10: Transmitting detonation wave from narrow gap to cylindrical chamber $[H_2] : [O_2] : [N_2] = 2 : 1 : 7$.

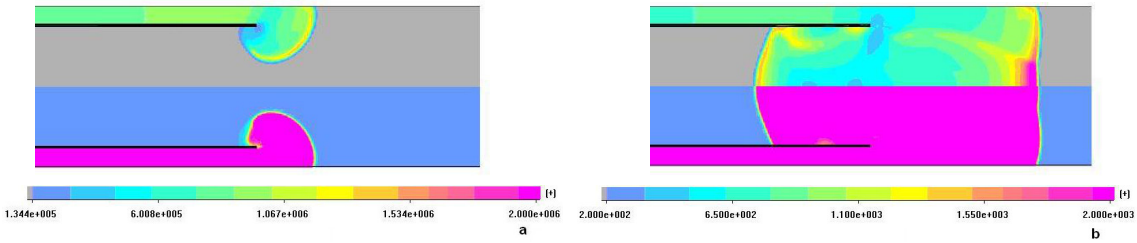

Figure 11: Transmitting detonation wave from narrow gap to cylindrical chamber $[H_2] : [O_2] : [N_2] = 2 : 1 : 5$. Mapping scales for pressure (a) and temperature (b).

because there are no reflected waves traveling from that side. It can be clearly traced from temperature maps, because temperature behind the transverse detonation wave increases close to its equilibrium value. Then convergence of shock waves to the axis of symmetry of the cylinder brings to an increase of its intensity and reinitiation of detonation upon reflection from the axis. Figure 12 illustrates more stages of transmission of a detonation wave in diluted stoicheometric mixture, which makes it possible to trace the mechanism of degeneration and reestablishing of detonation wave.

The result drives us to conclusions, that the suggested configuration is optimal for transmission detonation from narrow to wide chambers, and that developed numerical tool makes it possible to perform optimization studies of hydrogen - oxygen detonation engine design.

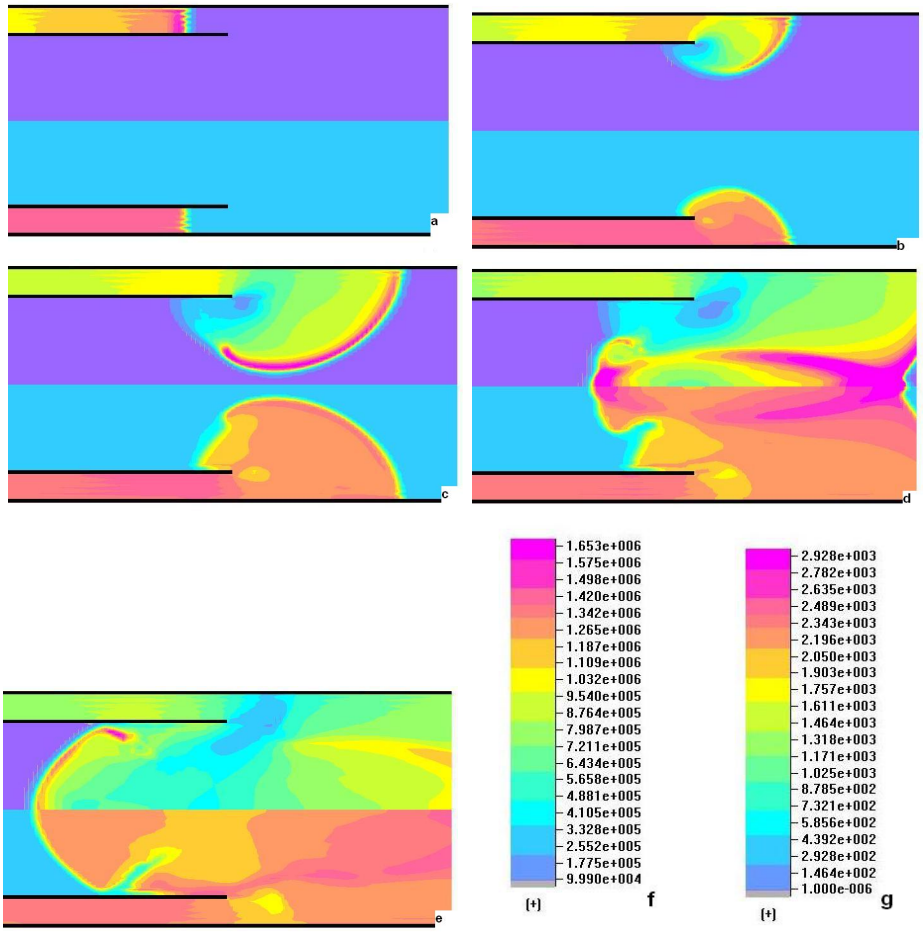

Figure 12: Transmitting detonation wave from narrow gap to cylindrical chamber $[H_2] : [O_2] : [N_2] = 2 : 1 : 6$. Times: a - 0.2448 ms, b - 0.2629 ms, c - 0.2707 ms, d - 0.2855 ms, e - 0.2978 ms, f,g - mapping scales for pressure (f) and temperature (g).

7 Conclusions

Detonation onset, decay and reinitiation in pulse detonation engines was studied numerically. The code resolves hydrogen combustion chemistry in a sufficient way to model anomalous behavior of ignition delay times versus pressure. Within one and the same solver it was made possible to model establishing slow diffusion and kinetic combustion modes, as well as onset of detonation modes. Verification and validation of the code were carried out.

Investigations showed that dependence of ignition delay time on pressure for hydrogen - oxygen mixtures is not monotonous and has three characteristic regions.

Ignition delay time generally increases for both rich and lean mixtures as compared with stoicheometric ones (under some conditions exceptions are possible).

Detonation degeneration and reestablishing on being transmitted from thin gap to a wide chamber was studied being relevant to pulse detonation engine functioning. It was demonstrated that on transmitting detonation from a narrow coaxial gap to a wide cylindrical chamber detonation wave degenerates but then could be reestablished due to cumulative energy effect in converging shock waves. While on transmitting expanding

detonation waves from a narrow tube into a wide tube detonation wave has much more chances to degenerate for the same mixture compositions.

Thus developed code makes it possible to simulate detonation onset and propagation in pulse detonation engines.

Acknowledgements.

The authors gratefully acknowledge financial support from the Russian Foundation for Basic Research (RFBR Grant 13-03-00003).

References

[1] Smirnov N.N., Pushkin V.N., Dushin V.R., Kulchitskiy A.V. Microgravity Investigation of Laminar Flame Propagation in Monodisperse Gas-Droplet Mixtures. Acta Astronautica, 2007, vol. 61, 626-636.

[2] Betelin V.B., Smirnov N.N., Dushin V.R., Nikitin V.F., Kushnirenko A.G., Nerchenko V.A., Evaporation and ignition of droplets in combustion chambers modeling and simulation, Acta Astronautica vol.70 (2012) pp. 23-35.

[3] V.R. Dushin, A.V. Kulchitskiy, V.A. Nerchenko, V.F. Nikitin, E.S. Osadchaya, Yu.G. Phylippov, N.N. Smirnov. Mathematical Simulation For Non-Equilibrium Droplet Evaporation. Acta Astronautica, 2008, vol. 63, pp 1360-1371.

[4] V.F. Nikitin, V.R. Dushin, Y.G. Phylippov, J.C. Legros. Pulse detonation engines: Technical approaches. Acta Astronautica 64 (2009) 281-287.

[5] Smirnov N.N., Nikitin V.F., Boichenko A.P., Tyurnikov M.V., Baskakov V.V. Deflagration to detonation transition in gases and its application to pulse detonation devices. In: Gaseous and Heterogeneous Detonations: Science to Applications (G.D.Roy et. al. Eds.) Moscow, ENAS Publ. 1999, pp.65-94.

[6] Smirnov N.N. and V.F.Nikitin, Comb. Exp. Shock Wave 40 (2):186-199, 2004.

[7] Smirnov N.N., Nikitin V.F., The Influence of Confinement Geometry on Deflagration to Detonation Transition in Gases. J. Phys. IV France, 12, Pr7, (2002) 341-351.

[8] N. N. Smirnov, V. F. Nikitin, S. Alyari Shurekhdeli. Investigation of Self-Sustaining Waves in Metastable Systems: Deflagration-to-Detonation Transition. Journal of Propulsion and Power, Vol. 25, No. 3, 2009 pp. 593-608.

[9] A. Linan, M. Bollig, A.L. Sanchez, B. Lazaro. Reduced kinetic mechanisms for modelling LPP combustion gas turbines. RTO AVT Symposium on Gas Turbine Engine Combustion, Emissions and Alternative Fuels. Lisbon, Portugal, 1998; RTO MP-14.

[10] Peters, N., and Williams, F.A. Combustion and Flame, 68, 1987, p. 185.

[11] Alexander Burcat: Third Millennium Ideal Gas and Condensed Phase Thermochemical Database for Combustion. Report TEA867, January 2001

[12] Maas, U., and Warnatz, J. Ignition process in hydrogen-oxygen mixtures. Combustion and Flame, 74, No. 1, 1988, pp. 53-69.

[13] U. Maas, and S.B. Pope. Simplifying chemical kinetics: intrinsic low-dimensional manifolds in composition space. Combustion and Flame, 88, 239-264 (1992).

[14] F.A. Williams. Short chemical mechanisms for deflagrations and detonations. Western States Section. The Combustion Institute Spring Meeting 2004, paper 04-S-1.

[15] R.J. Kee, J.A. Miller, and T.H. Jefferson. Chemkin: a general-purpose, problem-independent, transportable Fortran chemical kinetics code package. Sandia National Laboratories Report SAND80-8003 (1980).

[16] Gelfand B.E., Silnikov M.V., Medvedev S.P., Khomik S.V. Thermo- gas-dynamics of hydrogen combustion and explosion. St. Petersburg, Polytechnic Publ., 2009.

[17] Gelfand B.E., Popov O.E., Chaivanov B.B., Hydrogen: parameters of combustion and explosion. Moscow, PhysMathLit Publ. 2008.

[18] Philip M. Dissertation "Experimentelle und theoretische Untersuchungen zum Stabilitatsverhalten von Drallflammen mit zentraler Ruckstromzone". Karlsruhe University. 1991.

[19] Pironneau O. and Mohammadi B. Analysis of the K-Epsilon turbulence model. Masson Editeur, Paris, 1994.

N. N. Smirnov, V. F. Nikitin, Yu. G. Phylippov, Moscow M.V. Lomonosov State University, Moscow, Russia
N. N. Smirnov, V. F. Nikitin, Scientific Research Institute for System Analysis of the Russian Academy of Sciences, Moscow, Russia